research papers

Maximum-entropy-method charge densities based on structure-factor extraction with the commonly used Rietveld refinement programs *GSAS*, *FullProf* and *Jana2006*

Niels Bindzus and Bo Brummerstedt Iversen*

Center for Materials Crystallography, Department of Chemistry and iNANO, Aarhus University, Aarhus C., DK-8000, Denmark. Correspondence e-mail: bo@chem.au.dk

Structure-factor extractions in commonly used Rietveld refinement programs (*FullProf*, *Jana2006* and *GSAS*) were examined with respect to subsequent calculation of electron-density distributions (EDDs) using the maximum entropy method (MEM). As a test case, 90 K synchrotron powder X-ray diffraction data were collected on the potential hydrogen storage material, $NaGaH_4$, at SPring-8, Japan. To support the model, neutron powder diffraction data were collected on the fully deuterated sample at PSI, Switzerland. Firstly, it was established whether the programs can produce observed structure factors, F_{obs}, corrected for anomalous dispersion and scaled to the scattering power of one unit cell. Secondly, different models for background and peak-shape description were investigated with respect to the extracted F_{obs}, and the effect on the subsequent MEM EDDs was analysed within the quantum theory of atoms in molecules. Substantial differences are observed in the estimated standard deviations, σ_{obs}, produced by the different programs. Since σ_{obs} is a vital parameter in the calculation of MEM EDDs this leads to substantial variation between the MEM EDDs obtained with different Rietveld programs even in cases with similar F_{obs}. A new approach for selecting an optimized MEM EDD and thereby minimizing the effect of variation in σ_{obs} is suggested.

1. Introduction

Single-crystal X-ray diffraction data are generally considered to be more accurate than powder X-ray diffraction (PXRD) data because of inherent problems of extracting precise structure factors from powder data containing severe peak overlap. While this is probably true in many cases, it is not necessarily so for high-symmetry inorganic crystal structures. On the contrary, in these systems extinction effects can be severe in low-order single-crystal data due to high degrees of crystal perfection and, furthermore, twinning may be difficult to avoid. Furthermore, PXRD data can be collected in a single measurement, thereby rendering the scale of the different reflections identical. The huge number of scale factors used in typical single-crystal data is a significant problem for accurate electron-density distribution (EDD) studies and therefore PXRD data may be an attractive alternative. In the case of silicon and diamond, it has been shown that very accurate structure factors can be measured by synchrotron PXRD (Nishibori *et al.*, 2007). Svendsen *et al.* (2010) showed that these data on diamond had a quality suitable even for multipole electron-density modelling (Hansen & Coppens, 1978) and in a further analysis Fischer *et al.* (2011) strikingly showed that the data are of such outstanding quality that they revealed

polarization of the carbon core electrons. This in turn led to a revised multipole model, which explicitly takes core polarization into account. It is worth noting that the synchrotron PXRD data on diamond were collected in a matter of minutes to very high resolution, and that the derived multipole EDD was superior to the multipole EDD obtained from *Pendellösung* data (Spackman, 1991).

The maximum entropy method (MEM) has been used with great success in numerous studies based on synchrotron PXRD data (Takata *et al.*, 1995, 2001; Bentien *et al.*, 2000; Snyder *et al.*, 2004). The accuracy of the derived EDDs depends critically on the quality of the extracted structure factors based on the initial Rietveld refinement. In fact the success of extracting accurate structure factors from synchrotron PXRD data can be well understood. In conventional Rietveld refinement approaches, the structure factors are extracted from the powder data in accordance with an independent spherical atom model (ISAM). Thus, when individual structure factors are extracted from the observed intensities of overlapping reflections, the individual contributions from each structure factor to a measured data point are estimated from the ISAM (Rietveld, 1969). In this way an atomic bias is introduced in the extracted structure-factor values. However, since peak overlap is primarily a problem at

higher order, the low-order structure factors containing the majority of the bonding features are well determined even with an ISAM model. Hence, the aspherical bonding features are still included in the structure factors when an ISAM model is utilized for the extraction. In the case of diamond the use of aspherical electron-density models in the structure-factor extraction did not significantly improve the quality of the derived densities, although for more complex structures with peak overlap in the low-order data this will not be the case (Svendsen *et al.*, 2010). It is also worth noticing that for structures containing anharmonic thermal motion it will be more challenging to extract accurate structure factors, since anharmonic effects are most prominent in the high-order data, where the peak overlap is largest.

The fundamental idea behind the present study is to critically examine the ISAM structure-factor extraction from synchrotron PXRD data in commonly used Rietveld refinement programs: *FullProf* (Rodriguez-Carvajal, 1993), *Jana2006* (Petricek *et al.*, 2006) and *GSAS + EXPGUI* (Larson & Von Dreele, 1994; Toby, 2001). If reasonably accurate structure factors can be retrieved from typical PXRD data, then we envision that a much larger crystallographic community will overcome the barrier to go beyond ISAM crystal structures and also calculate MEM EDDs. The first aim of our study therefore is to investigate whether the commonly used Rietveld programs fulfil the requirement of the MEM input, which is a list of observed structure factors F_{obs} on an absolute scale and corrected for anomalous dispersion. Secondly, we examine which Rietveld refinement models provide the optimum set of F_{obs} and σ_{obs} for subsequent calculation of MEM EDDs. In this respect, different models for background and profile description are scrutinized. It should be emphasized that, in the case of non-overlapping peaks, accurate extraction of the observed integrated intensities depends primarily on the estimated background. We note again that many studies already have calculated MEM EDDs based on synchrotron PXRD data, and that these have been used to discuss *e.g.* disorder, integrated atomic charges and topological features (Gilmore, 1996; Bagautdinov *et al.*, 1998; Dinnebier *et al.*, 1999; Noritake *et al.*, 2003; Nishibori *et al.*, 2007; Samy *et al.*, 2010; Buchter *et al.*, 2011). Our goal is to bring such studies on a more common footing.

As proof of principle we present Rietveld refinements and MEM EDDs based on 90 K synchrotron PXRD data measured on the potential hydrogen storage material $NaGaH_4$. This can be considered a typical material of both fundamental and technological interest, and thus a typical example of the type of studies that may be done using the present approach. The crystal structure of $NaGaH_4$ consists of almost isolated GaH_4^- anions and spherical Na^+ moieties placed in an orthorhombic lattice. In the centrosymmetric space group *Cmcm* (63), there are two non-equivalent H atoms (Irodova *et al.*, 1989; Nozik *et al.*, 1991). In the literature there are two reports on $NaGaH_4$ using *ab initio* density functional theory (DFT) calculations (Vajeeston *et al.*, 2004; Herbst *et al.*, 2010), and these predict a non-metallic character with a finite band gap of ~ 5 eV and a standard enthalpy of

formation, $\Delta H_{298K} \sim -30$ kJ mol^{-1} H$_2$. The synchrotron PXRD data were collected at 90 K at SPring-8, Japan, while corresponding neutron data were collected on a fully deuterated sample at PSI, Switzerland, to obtain more accurate structural parameters for hydrogen using the $X-N$ procedure (Coppens, 1967; Iversen, Larsen *et al.*, 1997; Overgaard *et al.*, 1999, 2001; Macchi *et al.*, 2000). For both the neutron and the X-ray diffraction cases multi-temperature data were collected, but the full analysis of all data sets will form the basis for a future report focusing on the chemical properties of the material.

2. Experimental

2.1. X-ray powder diffraction

A powder sample of $NaGaH_4$ was synthesized according to a procedure described in the literature (Bakum & Ereshko, 1977). High-resolution PXRD data at 90 K were collected at beamline BL02B2 at the SPring-8 synchrotron facility in Japan. The white, air-sensitive powder sample was mounted in a capillary in the large image-plate Debye–Scherrer camera (Nishibori *et al.*, 2001). The camera is capable of rapidly collecting PXRD data, which are suitable for charge-density studies due to high counting statistics and high angular resolution. A CeO_2 standard ($a = 5.41110$ Å) was used to determine the synchrotron radiation wavelength, $\lambda = 0.481496$ (2) Å. Owing to the high energy of the X-rays, the angular variation of absorption with diffraction angle becomes less than 0.5%, and absorption correction is therefore ignored in the present study. The temperature was controlled by an N_2 gas flow system.

2.2. Neutron powder diffraction

A fully deuterated sample, $NaGaD_4$, was synthesized by a similar procedure (Bakum & Ereshko, 1977). In a glovebox, 1 g of the sample was placed in a vanadium cylinder with an outer diameter of 6 mm and this was subsequently tightly closed with a lead seal. Neutron powder diffraction data were measured at 90 K at the Swiss Spallation Neutron Source at PSI using the high-resolution powder diffractometer for thermal neutrons (Fischer *et al.*, 2000). The wavelength was chosen to be 1.1545 Å and the diffracted beam was detected by a large position-sensitive ^{3}He detector with angular step of 0.1°. The temperature was controlled by a cryostat. Based on the NIST's scattering length density calculator (http://www.ncnr.nist.gov/resources/sldcalc.htm), the absorption correction was estimated to be $\mu R = 0.027$.

2.3. Rietveld refinement

In order to facilitate comparison between the three Rietveld programs, their set-ups were simplified and made as identical as possible. The polarization correction was selected to be that of a linearly polarized beam, and the low asymmetry of the PXRD data allowed for the omission of asymmetry in the peak-shape models. Form factors were determined by the analytic expressions given in *International Tables for Crys-*

tallography Volume C (Table 6.1.1.4, 3rd edition). The input anomalous dispersion parameters were determined with the program *FPrime* (Von Dreele, 1994) to be $f'(Na) = 0.009$, $f''(Na) = 0.011$, $f'(Ga) = 0.236$ and $f''(Ga) = 0.807$. The structural refinement was improved relative to published models (Irodova *et al.*, 1989; Nozik *et al.*, 1991) by fixing the hydrogen positional and heavy atom scaled atomic displacement parameters (ADPs) obtained from Rietveld refinement on the $NaGaD_4$ neutron powder data at fixed values. Diffractograms of all Rietveld refinements are provided in the supplementary material.[1] From all refinements, an output of 191 observed structure factors corresponding to a resolution of $\sin(\theta/\lambda) = 0.62$ Å^{-1} was obtained. In *Jana2006* the required output information was provided by 'BayMEM' files, in *Full-Prof* by 'fou' files defined by the program label of -1. In *GSAS* two types of observed structure factors, designated *FOT* and *FO* in the manual, were extracted utilizing the *REFLIST* routine.

3. Structure-factor analysis in *FullProf, Jana2006* and *GSAS*

3.1. Anomalous dispersion and absolute scale

Since F_{MEM} is determined by a discrete Fourier transformation of ρ, a number of requirements are imposed on the experimental data, F_{obs}. In particular, they must be on an absolute scale and corrected for the effects of anomalous dispersion (AD) and extinction. The latter is, for practical purposes, avoided if the powder sample is very finely grained. Thus, the focus of this section is on how the Rietveld programs handle the two other requirements.

The scale of the extracted F_{obs} can easily be checked through the (000) reflection which, for absolute scaling, equals the number of electrons in one unit cell. Based on the extracted structure factors from the three programs it is concluded that this is fulfilled in *Jana2006* and *FullProf*. In *GSAS* $F_{obs}(FOT)$ is on a lower scale and $F_{obs}(FO)$ is on a considerably higher scale.

It is investigated whether or not the Rietveld programs correct the extracted F_{obs} for AD. Based on the different output formats described in §2.3, we have in Fig. 1 plotted the structure-factor difference

$$\Delta F_{obs}(\mathbf{H}_i) = \left|F_{obs}^{AD}(\mathbf{H}_i)\right| - \left|F_{obs}^{0}(\mathbf{H}_i)\right|, \tag{1}$$

where F_{obs}^{AD} are the extracted, observed structure factors obtained on the basis of a refinement model that describes AD. In the case of F_{obs}^{0} the structure-factor extraction has been accomplished with an identical refinement model only deviating in terms of the AD parameters, which have been set equal to zero. If the Rietveld program does not correct for AD in the output file, then $\left|F_{obs}^{AD}(\mathbf{H}_i)\right| \simeq \left|F_{obs}^{0}(\mathbf{H}_i)\right|$ and $\Delta F_{obs}(\mathbf{H}_i)$ fluctuates around zero. It will not be perfectly zero as the decomposition of overlapping reflections is model dependent.

If the Rietveld program correctly removes the AD contribution, then an approximate agreement with the calculated reference, $\Delta F_{ref}(\mathbf{H}_i)$, is anticipated. The reference is absolutely scaled and based on model calculations with and without the AD taken into account; detailed information is found in the supplementary material. Consequently, from Fig. 1 it can be deduced that both *Jana2006* and *GSAS(FOT)* deliver F_{obs} corrected for the AD contribution, whereas no AD correction has been performed in *FullProf* and *GSAS(FO)*.

From this point on, the investigated output of *GSAS* is limited to $F_{obs}(FO)$ since in *GSAS* it is the only type of structure factor for which standard deviations are provided. Furthermore, post-modification cannot be avoided in *GSAS* as both $F_{obs}(FOT)$ and $F_{obs}(FO)$ are not absolutely scaled.

3.2. Background modelling

MEM EDDs based on synchrotron PXRD data are sensitive to the selected background approximation applied in the least-squares refinement. The high resolution of synchrotron PXRD enables a reliable estimation of the background between the diffraction peaks, thereby rendering interpolation an appropriate choice for describing the background in these kinds of data. Hence, we performed refinement series in *Jana2006* and *FullProf* with a progressively improved selection of background points, from which the background is approximated by linear interpolation. Further improvement in the background modelling was obtained by combining linear interpolation with smoothing techniques included in the refinement software. A different approach was employed for *GSAS* as it applies linear interpolation in an alternative way. Here, it is only required to state a number of terms, N, which
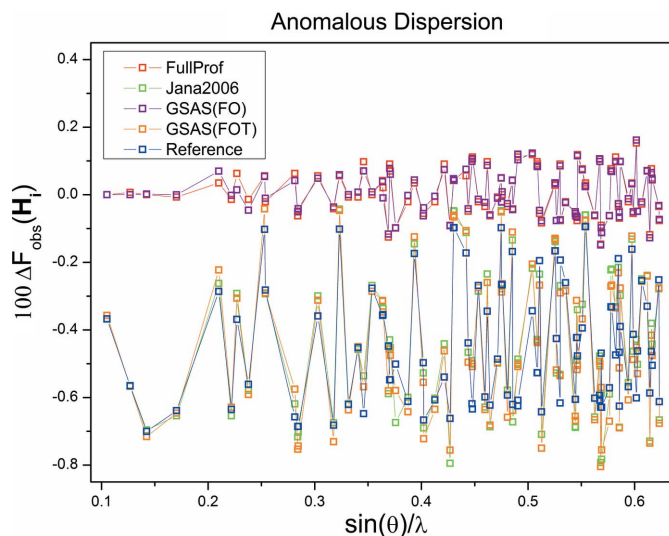
Figure 1
Plot of the difference $\Delta F_{obs}(\mathbf{H}_i) = \left|F_{obs}^{AD}(\mathbf{H}_i)\right| - \left|F_{obs}^{0}(\mathbf{H}_i)\right|$ in each Rietveld program for structure factors with a phase of zero. For each set of extracted F_{obs}, the scale is set relative to the F_{obs} of the strong (200) reflection. The reference line corresponds to what we believe is the correct AD contribution, although it does not include the effect of decomposition of overlapping reflections.

Table 1
Overview of lattice parameters (Å), fractional coordinates and isotropic ADPs (Å^2) for the Rietveld refinements with varying background approximation performed in *FullProf* (F1–3), *Jana2006* (J1–3) and *GSAS* (G1–2).

Agreement factors for the refinements are defined by $R_p = 100[(\sum |y_i - y_{\mathrm{calc},i}|)/\sum y_i]$, $R_{wp} = 100\{[\sum \sigma_i^{-2}(y_i - y_{i,\mathrm{calc}})^2]/\sum \sigma_i^{-2} y_i^2\}^{1/2}$ and $R_F = 100\{[\sum |F_{\mathrm{obs}}(\mathbf{H}) - F_{\mathrm{calc}}(\mathbf{H})|]/\sum |F_{\mathrm{obs}}(\mathbf{H})|\}$; y is the intensity count and F are structure factors corrected for AD. The modified goodness-of-fit parameter, S^2, is defined in equation (3). Agreement factors for computed MEM EDDs are expressed as $R_{\mathrm{MEM}} = 100\{[\sum |F_{\mathrm{obs}}(\mathbf{H}) - F_{\mathrm{MEM}}(\mathbf{H})|]/\sum |F_{\mathrm{obs}}(\mathbf{H})|\}$ and $R_{\mathrm{wMEM}} = 100\{[\sum \sigma^{-2}(\mathbf{H})|F_{\mathrm{obs}}(\mathbf{H}) - F_{\mathrm{MEM}}(\mathbf{H})|^2]/\sum \sigma^{-2}(\mathbf{H})|F_{\mathrm{obs}}(\mathbf{H})|^2\}^{1/2}$. The atomic charges (e) and the density at the BCPs (e Å^{-3}) are obtained from topological analysis.

	F1	F2	F3	J1	J2	J3	G1	G2
a	7.0271 (1)	7.0272 (1)	7.0271 (1)	7.0272 (2)	7.0272 (2)	7.0272 (2)	7.0272 (1)	7.0271 (2)
b	6.4605 (1)	6.4605 (1)	6.4605 (1)	6.4606 (2)	6.4606 (2)	6.4606 (2)	6.4606 (1)	6.4606 (2)
c	7.0396 (1)	7.0396 (1)	7.0396 (1)	7.0396 (2)	7.0396 (2)	7.0396 (2)	7.0397 (1)	7.0397 (2)
y(Na)	0.3442 (5)	0.3444 (5)	0.3442 (4)	0.3442 (4)	0.3444 (4)	0.3444 (4)	0.3442 (4)	0.3439 (5)
B_{iso}(Na)	0.98 (6)	0.96 (6)	0.96 (5)	0.98 (6)	0.96 (5)	0.96 (6)	0.68 (5)	0.71 (6)
y(Ga)	−0.1589 (2)	−0.1588 (2)	−0.1589 (2)	−0.1589 (2)	−0.1588 (2)	−0.1588 (2)	−0.1581 (2)	−0.1585 (2)
B_{iso}(Ga)	0.46 (3)	0.46 (3)	0.47 (2)	0.46 (2)	0.45 (2)	0.45 (2)	0.40 (2)	0.36 (2)
R_F	1.49	1.34	1.19	1.97	1.84	1.75	1.95	1.98
R_p	1.08	1.02	1.08	1.11	1.00	1.00	1.23	1.27
R_{wp}	1.74	1.69	1.71	1.78	1.66	1.66	1.90	1.94
S^2	20.2	19.6	11.1	3.75	3.32	3.03	11.5	11.0
MEM electron-density distribution								
R_{MEM}	0.50	0.50	0.48	1.06	1.06	1.05	1.05	1.09
R_{wMEM}	0.34	0.34	0.33	1.25	1.24	1.24	1.26	1.26
Q_{Na}	0.72	0.77	0.55	0.76	0.73	0.72	1.05	1.11
Q_{Ga}	0.90	0.79	0.99	0.68	0.62	0.57	1.68	1.69
Q_{H1}	−0.09	−0.10	−0.09	−0.24	−0.31	−0.31	−0.46	−0.44
Q_{H2}	−0.30	−0.35	−0.41	−0.35	−0.32	−0.33	−0.51	−0.32
Q_{NaGaH4}	0.84	0.65	0.54	0.25	0.05	0.03	0.78	1.27
$\rho_{\mathrm{BCP}}^{\mathrm{Ga-H1}}$	0.76	0.74	0.73	0.65	0.63	0.65	0.83	0.79
$\rho_{\mathrm{BCP}}^{\mathrm{Ga-H2}}$	0.58	0.56	0.54	0.48	0.50	0.50	0.54	0.63

equals the number of adjustable background parameters, and this is utilized to partition the powder scan range into $N - 1$ equally 2θ-spaced segments. Thus, the accuracy of this approach is limited as it impedes a careful selection of background points. For comparative reasons two refinements utilizing different background models were performed in *GSAS*. In all three refinement programs the peak shape was modelled with the Thompson–Cox–Hastings pseudo-Voigt function (Thompson *et al.*, 1987).

In the first *FullProf* refinement, F1, 56 points were automatically selected and subsequently optimized by refining their intensity height. In the following refinement, F2, the background description was ameliorated by manually selecting 84 points, which similarly were optimized by refining their intensity height. The additional points are predominantly located at the beginning of the diffractogram. Finally, in F3 a smoother background approximation is fabricated by applying an iterative Fourier filtering technique (Press *et al.*, 1992) to the final background description obtained in F2. The background modelling of the two *Jana2006* refinements, J1 and J2, was manufactured by importing the final background points of F1 and F2, respectively. These points were kept fixed during refinement in *Jana2006*. In J3 the background approximation is made smoother by combining the imported linear interpolation description utilized in J2 with a Legendre polynomial consisting of 23 adjustable coefficients. Two refinements denoted G1 and G2 were carried out in *GSAS*. In G1 the

background is modelled by linear interpolation utilizing $N = 36$, which is the maximal allowed number of adjustable parameters. This background function only provides a crude approximation of the wavy background observed in the PXRD data; therefore, an additional background model is investigated in G2. Here, a Chebyshev polynomial consisting of 27 adjustable parameters is employed; however, also in this case an inadequate background approximation is obtained.

The refined structural parameters obtained with *Jana2006* and *FullProf* are statistically equal, whereas those refined in *GSAS* deviate for the isotropic thermal motion parameters (see Table 1). This is a consequence of the rather crude background description produced in *GSAS*. According to the agreement factors, the *FullProf* refinements give the best fit between data and the structural model, whereas the R_F values of the corresponding *Jana2006* refinements are considerably larger and even similar to those of G1–2. This results from the lacking option of co-refining the profile parameters and linear interpolation parameters in *Jana2006*. Owing to model bias the similar R_F values of J1–3 and G1–2 ought to be carefully interpreted; however, the considerably lower R_p values of J1–3 illustrate that the *Jana2006* refinements fit the data more tightly. Furthermore, the differences between J1–2 and F1–2 reflect the fact that the programs' profile function is not exactly equal, even though both of them are based on the Thompson–Cox–Hastings pseudo-Voigt function.

Table 2
Inter-data-set agreement factor, $R(i,j) = \sum ||F_{obs}^i| - |F_{obs}^j|| / \sum |F_{obs}^i|$, and the average, $\langle i,j \rangle = \langle |F_{obs}^i| / |F_{obs}^j| \rangle$.

R(F3, F1)	0.65	$\langle$F3, F1$\rangle$	0.996
R(F3, F2)	0.57	$\langle$F3, F2$\rangle$	0.996
R(J3, J1)	0.41	$\langle$J3, J1$\rangle$	1.001
R(J3, J2)	0.23	$\langle$J3, J2$\rangle$	1.001
R(G1, G2)	1.38	$\langle$G1, G2$\rangle$	0.991
R(J3, F3)	1.29	$\langle$J3, F3$\rangle$	0.998
R(J3, G1)	3.37	$\langle$J3, G1$\rangle$	0.980
R(J2, F2)	1.18	$\langle$J2, F2$\rangle$	0.993

Further comparison can be made by comparing the F_{obs} extracted from different refinements utilizing plots of $|F_{obs}^i| / |F_{obs}^j|$ as well as an appertaining average, $\langle i,j \rangle$, and an inter-data-set agreement factor, $R(i,j)$ (see Fig. 2 and Table 2). For the *Jana2006* refinements addition of the Legendre polynomial to the linear interpolation background leads to

significant changes, especially at higher angles. In *FullProf* considerable changes are observed both at low and high angles. This is probably due to the higher flexibility of the Fourier filtering technique. Similarly, the two *GSAS* refinements also differ considerably at both low and high angles, and as seen from the value of R(G1, G2) the magnitude of these differences is on average substantially larger than those internally observed in *FullProf* and *Jana2006*. The remaining plot in Fig. 2 compares the observed structure factors between the programs. The J3/G1 relationship illustrates that the *GSAS* output differs considerably from those of *Jana2006* and *FullProf*, especially for the F_{obs} originating from weak high-order reflections. The differences of the much more similar outputs of *FullProf* and *Jana2006* are elaborated by calculating residual EDDs, ρ_{res}, of F3 and J3 (see Fig. 3). In the charge-density field these are also coined dynamic deformation densities. Both residual densities have similar deformation features at the Na and Ga sites, and they also indicate weak interactions
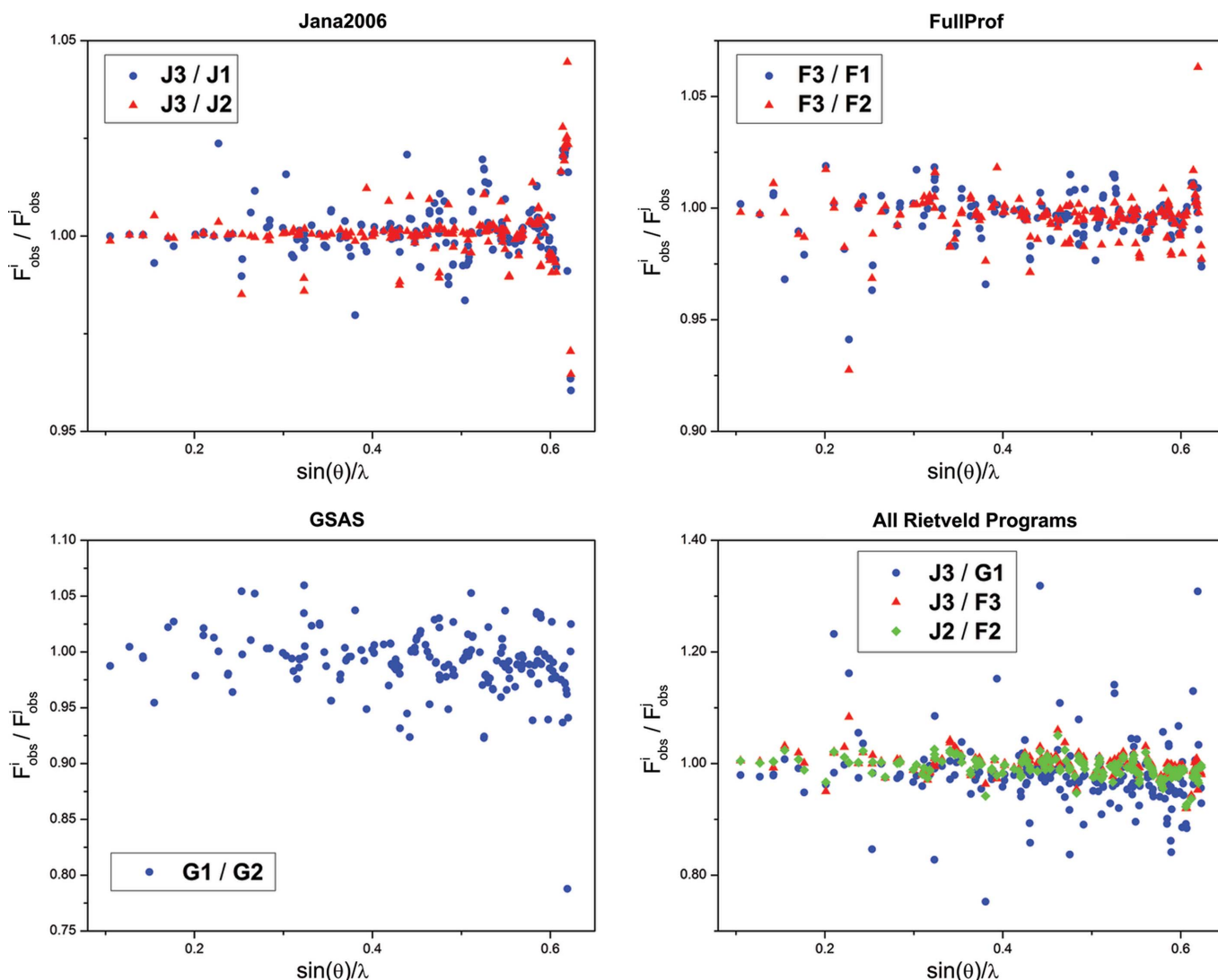
Figure 2
Analysis of the extracted observed structure factors in the three Rietveld programs through their dependency on the background description. The last plot compares the extracted $F_{obs}(\mathbf{H})$ between the programs. Prior to the comparison, the output files of *GSAS* and *FullProf* were subjected to post-treatment in *XD2006* in order to correct for AD. In addition this also brings the *GSAS* output onto an absolute scale.

Table 3
Overview of lattice parameters (Å), fractional coordinates and isotropic ADPs (Å^2) for Rietveld refinements performed in *FullProf*, FP1–4, in which the profile modelling is varied.

Agreement factors are defined in Table 1.

	FP1	FP2	FP3	FP4
a	7.0271 (2)	7.0272 (1)	7.0274 (1)	7.0261 (3)
b	6.4605 (2)	6.4605 (1)	6.4606 (1)	6.4602 (3)
c	7.0396 (2)	7.0396 (1)	7.0394 (1)	7.0409 (3)
$y(\text{Na})$	0.3443 (5)	0.3444 (5)	0.3443 (5)	0.3441 (8)
$B_{\text{iso}}(\text{Na})$	0.95 (6)	0.96 (6)	0.97 (6)	0.81 (9)
$y(\text{Ga})$	−0.1588 (2)	−0.1588 (2)	−0.1588 (2)	−0.1587 (3)
$B_{\text{iso}}(\text{Ga})$	0.42 (2)	0.46 (3)	0.45 (3)	0.38 (3)
R_F	1.27	1.34	1.47	1.27
R_{p}	1.03	1.02	1.00	1.48
R_{wp}	1.70	1.69	1.64	2.97

between hydrogen and its neighbouring atoms, *e.g.* the H1$\cdots$H1 in the (200) plane. Hence, they agree qualitatively, but the scale of the residual features is considerably larger in the case of J3. This agrees with the higher R_F value of J3 (Table 1). The effect of the difference between the profile functions of *Jana2006* and *FullProf* can be estimated by comparing a *FullProf* and *Jana2006* refinement with equal background modelling, *e.g.* F2 and J2 in Fig. 2. The value of $R(\text{J2}, \text{F2})$ shows that the profile differences on average give rise to larger changes in the observed structure factors than the modifications of the background description in both F1–3 and J1–3.
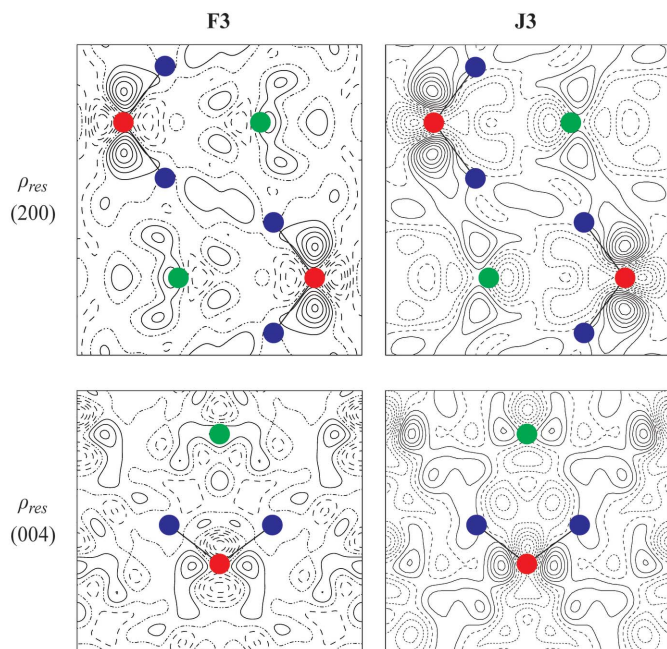
Figure 3
Residual EDDs for the Rietveld refinements F3 and J3 which are calculated by inverse Fourier summation of the difference $\Delta F = F_{\text{obs}} - F_{\text{calc}}$. The contour lines are at 0.05 and 0.08 e Å^{-3} for F3 and J3, respectively. Dotted lines represent negative values and solid lines positive values. Ga (red), Na (green) and H (blue).

Significant changes in the extracted F_{obs} are demonstrated for the refinement series with progressively improved background approximation, F1–3 and J1–3. In the ensuing sections it is illustrated that these changes result in distinctly different MEM EDDs. As a consequence of the inadequate background approximation, the MEM EDDs based on G1 and G2 are anticipated to be inferior compared with those of F1–3 and J1–3.

3.3. Peak shape

The decomposition of overlapping reflections in PXRD data depends on the selected peak-shape model. Therefore, an appropriate model choice is crucial for the F_{obs} extraction and the subsequent MEM EDD. Our analysis is confined to *FullProf*, since this software offers a wide selection of peak-shape models. Among the possible models, we focus on four relevant models: pseudo-Voigt (FP1), Thompson–Cox–Hastings pseudo-Voigt (FP2), Pearson VII (FP3) and a Lorentzian (FP4). The latter is the simplest model and inferior to the others, especially in the description of low-order reflections. However, as single peaks dominate this region, the impact of the peak-shape differences is minimized. Thus, FP4 may be able to extract F_{obs} similar to those of FP1–3. In the Rietveld refinements FP1–4 the background approximation is accomplished by linear interpolation utilizing points located at 2θ positions identical to those of the F2 refinement (see §3.2). As a consequence of this approach, FP2 equals F2. Owing to the high correlation with the chosen peak-shape model, the intensity height of the background points is refined in each refinement.

The refined structural parameters obtained in FP1–3 are statistically equal, whereas those refined in FP4 especially deviate for the isotropic ADPs (see Table 3). According to the agreement factors, FP1 gives the best fit between data and model. In FP2–4 the model fit gradually becomes worse, but even the R_F value of FP4 seems reasonable. As anticipated, the R_{p} values demonstrate that FP4 inferiorly describes the collected diffractogram compared with FP1–3.

Further analysis is performed by comparing the F_{obs} extracted from FP1–4 utilizing plots of $|F_{\text{obs}}^i|/|F_{\text{obs}}^j|$ as well as an appertaining average, $\langle i, j \rangle$, and inter-data-set agreement factor, $R(i, j)$ (see Fig. 4 and Table 4). Here, it is seen that the majority of F_{obs} modifications occur in the high-order region, *i.e.* the region dominated by overlapping reflections. In the low-order region much smaller differences are observed, but even single peaks have differences due to correlation with the background approximation. FP4 extracts low-order F_{obs} similar to FP1–3; however, considerable differences are observed in the high-order region despite the improved peak-shape modelling. These high-order differences originate from the substantially lower ADPs of FP4. Furthermore, the extracted F_{obs} of FP1 are predominantly larger than those of FP2–3 due to the smaller ADPs, whereas no systematic features are observed in the differences between the F_{obs} of FP2 and FP3. On average, FP2 and FP3 are more similar than FP1 and FP2. The overall similarity, especially at low order,
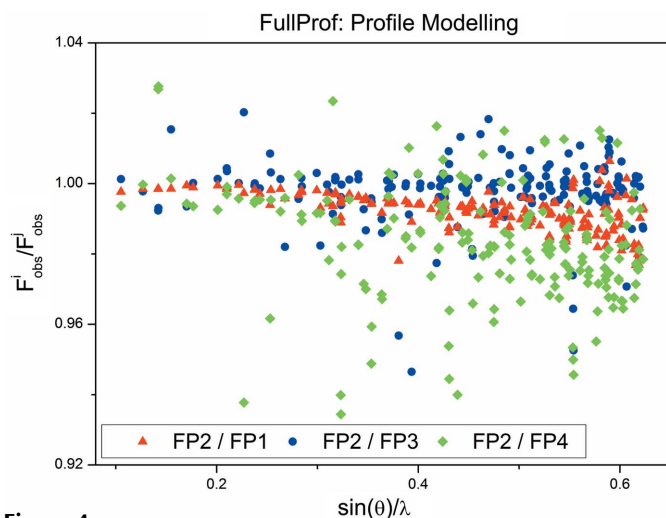
Table 4
Inter-data-set agreement factor, $R(i,j) = \sum ||F^i_{\mathrm{obs}}| - |F^j_{\mathrm{obs}}|| / \sum |F^i_{\mathrm{obs}}|$, and the average, $\langle i,j \rangle = \langle |F^i_{\mathrm{obs}}|/|F^j_{\mathrm{obs}}| \rangle$.

R(FP2, FP1)	0.73	$\langle$FP2, FP1$\rangle$	0.992
R(FP2, FP3)	0.40	$\langle$FP2, FP3$\rangle$	0.997
R(FP2, FP4)	1.73	$\langle$FP2, FP4$\rangle$	0.982

between FP1 and 4 implies that all four sets of F_{obs} will result in MEM EDDs with similar valence features. This is explored by calculating residual EDDs (see Fig. 5), where similar density deformation at the Na and Ga sites as well as weak electron accumulation between H···Na and H···Ga are observed. Hence, FP1–4 result in qualitatively identical pictures of the structure even though there are significant differences between the structure factors. The quantitative analysis in the subsequent section is restricted to the refinements with varying background approximation (Table 1), as the analysis on FP1–4 provides observations and conclusions similar to those of F1–3.

4. Electron densities

MEM EDDs of all the refinements with varying background approximations, see Table 1, were calculated using the *BayMEM* software (van Smaalen *et al.*, 2003), in which the Sakata–Sato algorithm was selected (Sakata & Sato, 1990). A relatively fine pixel grid of $144 \times 128 \times 144$ was used along the crystallographic axes a, b and c, corresponding to a pixel size of ~0.05 Å, in order to reduce errors due to a finite grid (van Smaalen & Netzel, 2009). MEM artefacts resulting from series-termination effects (Jauch, 1994; de Vries *et al.*, 1996; Iversen, Jensen & Danielsen, 1997; Bentien *et al.*, 2000) are minimized by using a procrystal prior based on the relevant refined model. Based on the assumption of a Gaussian distribution of errors, the MEM EDD is constrained to the

scattering data through the so-called F constraint (Sakata & Sato, 1990):

$$C_F = -\chi^2_{\mathrm{aim}} + \frac{1}{N_F} \sum_{i=1}^{N_F} \left(\frac{|F_{\mathrm{obs}}(\mathbf{H}_i) - F_{\mathrm{MEM}}(\mathbf{H}_i)|}{\sigma(\mathbf{H}_i)} \right)^2 = 0, \quad (2)$$

where $F_{\mathrm{obs}}(\mathbf{H}_i)$ is the observed structure factor of the Bragg reflection with scattering vector $\mathbf{H}_i$ and $\sigma(\mathbf{H}_i)$ is its standard uncertainty.

$F_{\mathrm{MEM}}(\mathbf{H}_i)$ is determined by a discrete Fourier transformation of the MEM EDD, and N_F is the number of reflections for which experimental structure factors, $F_{\mathrm{obs}}(\mathbf{H}_i)$, are available. Convergence for the iterative MEM procedure is obtained when $C_F \leq 0$. To facilitate the frame of reference, the convergence criterion is consistently set to the standard value $\chi^2_{\mathrm{aim}} = 1.0$, and no further MEM enhancements such as static weighting (de Vries *et al.*, 1994; Iversen *et al.*, 1995) are employed. Prior to the application of the MEM, the output files of *GSAS* and *FullProf* were subjected to necessary post-treatment in *XD2006* as discussed in §3.1.

In Table 1 results from topological analysis of the EDDs are provided (Bader, 1994). The atomic charges, Q, reveal that charge is transferred to the H atoms from Na and Ga. With improving background modelling, the noise and artefact levels are reduced in the EDDs, and as a consequence the atomic charges gradually come closer to fulfilling the electroneutrality condition. However, only the J2 and J3 EDDs fully comply with electroneutrality (0.05 and 0.03 e, respectively). Despite the thermally smeared nature of MEM EDDs, all the densities

Figure 4
Analysis of observed structure factors extracted from the *FullProf* refinements FP1–4 which differ in peak-shape model. Prior to the comparison, the output files of *FullProf* were subjected to post-treatment in *XD2006* in order to correct for AD.
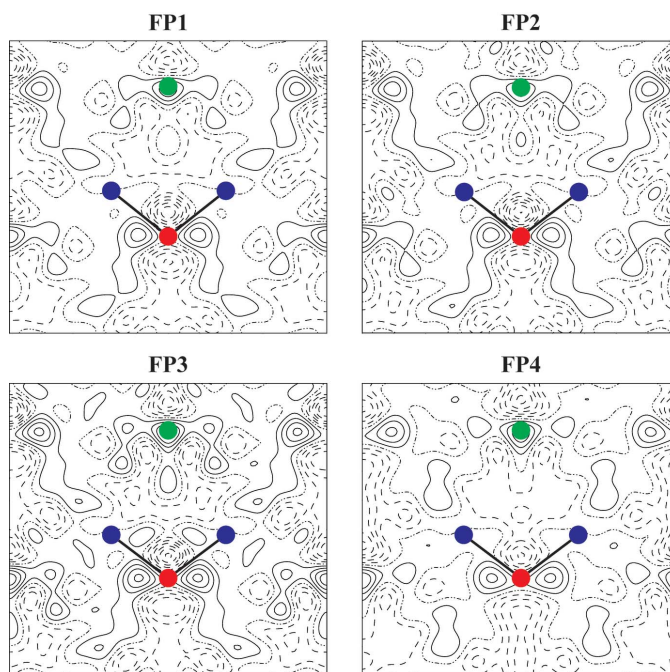

Figure 5
Residual EDDs, ρ_{res}, for the Rietveld refinements FP1–4 computed by inverse Fourier summation of the difference $\Delta F = F_{\mathrm{obs}} - F_{\mathrm{calc}}$. The (004) section is illustrated with contour lines at 0.05 e Å^{-3}. Dotted lines represent negative values and solid lines positive values. Ga (red), Na (green) and H (blue).

are capable of describing the H atoms in terms of a bond-critical point (BCP) between the Ga and H atom and a local atomic maximum. As anticipated, the topologies of the G1 and G2 EDDs deviate appreciably from those of F1–3 and J1–3. However, significant differences are also found between the EDDs of J1–3 and F1–3. This is quite surprising in the case of the refinements with equivalent background description. The differences originate from the software-dependent estimation procedure of σ_{obs}, which is a subject discussed further below. The considerable variation in the charges and the density values at the BCPs emphasizes the importance of a high-quality background approximation for MEM EDDs based on PXRD data.
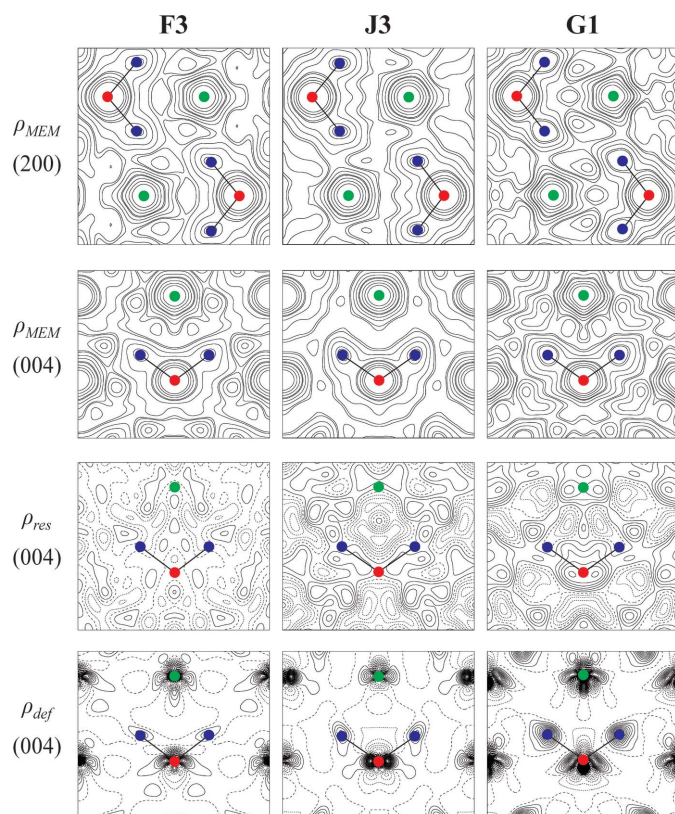
To analyse further the differences between the programs, one EDD from each refinement program along with corresponding MEM residual maps (inverse Fourier summation of $F_{obs} - F_{MEM}$) and dynamic MEM deformation densities ($\rho_{MEM} - \rho_{prior}$) are shown in Fig. 6. For each program the MEM EDD was selected as the one best fulfilling electroneutrality for the topological atoms. The density distribution through the Ga—H1 and Ga—H2 bonds as well as neigh-

bouring Na atoms can be observed in the plots of the (200) and (004) sections. Besides the clear features of the atoms and covalent bonds, the MEM EDDs also illustrate weak interactions between various atoms such as H1···H1 and H···Na. These interactions are also implied by the residual plots of the Rietveld refinements (see Fig. 3). In particular, the MEM EDD of G1 shows significant artefacts in terms of electron accumulation between Ga and Na. The noise level is estimated from the highest density values of the non-nuclear maxima, which for the G1, F3 and J3 EDDs are 0.22, 0.34 and 0.07 e Å^{-3}, respectively. The fit between the diffraction data and the MEM density is shown in the MEM residual maps, where it is apparent that the F3 distribution is significantly flatter than those of G1 and J3. This implies that in the reconstruction of the F3 EDD, the diffraction data have been substantially over-fitted. Support for this is found in the higher ρ_{BCP} values as well as the substantially lower R_{MEM} and R_{wMEM} values compared with the J3 and G1 EDDs. This is also the reason for the relatively high noise level observed in the F3 EDD. For the G1 and J3 EDDs it is less clear whether they over- or under-fit the diffraction data. In the residual densities unfitted structure is seen at the atomic positions and along the Ga—H bond, but it is difficult to precisely determine the location of noise areas, and it is therefore impossible to estimate whether the structure has been fitted down to the noise level. The optimal MEM stopping criteria for the individual refinements are further discussed below. The dynamic MEM deformation densities all have similar features such as added density to hydrogen sites and polarization of the atomic electron density of Na and Ga. Furthermore, an interesting feature is observed in the polarized densities of Na and Ga, which point directly towards each other in the F3 and J3 EDDs.

The results from the J1–3 refinements demonstrate that linear interpolation background modelling is sufficient to produce reasonable MEM EDDs, and that further improvements can be obtained by introducing smoothing schemes. The same conclusions apply to the F1–3 EDDs, but these densities have been over-fitted due to poor estimation of σ_{obs}, which leads to a wrong MEM stopping criterion. The G1–2 refinements lack flexibility in order to sufficiently describe the wavy background of the PXRD data. Consequently, the resulting MEM EDDs are not close to complying with electroneutrality, and they deviate significantly from those of J1–3 and F1–3.

Figure 6
Comparison of MEM EDDs, ρ_{MEM}, obtained after structure-factor extraction with the three Rietveld refinement programs. The first two rows illustrate the tetrahedral bonds in the GaH$_4$ unit by plotting ρ_{MEM} in the (200) and (004) sections; Ga—H1 is observed in (200), whereas Ga—H2 is seen in (004). Contour levels are defined by $2^x \times 10^y$; $x = 0, 1, 2, 3$ and $y = -2, -1, 0$. The last two rows contain MEM residual maps (ρ_{res}, contour level of 0.04 e Å^{-3}) and dynamic MEM deformation densities (ρ_{def}, contour level 0.1 e Å^{-3}) in the (004) plane. Ga (red), Na (green) and H (blue).

4.1. Estimated uncertainties

In the previous section, the analysis of the MEM EDDs demonstrated considerable differences. Surprisingly even the *FullProf* and *Jana2006* refinements with identical background modelling gave quite large differences in the MEM EDDs. As shown in Fig. 2 the extracted structure factors from *Jana2006* and *FullProf* are almost identical. The observed differences must therefore be attributed to different estimation procedures for the standard uncertainties. For each Rietveld program, this is explored by plotting the significance, F_{obs}/σ_{obs},

and calculating a modified goodness-of-fit parameter, S, defined by

$$S^2 = \frac{1}{N_{ref}} \sum_{i=1}^{N_{ref}} \left(\frac{|F_{obs}(\mathbf{H}_i)| - |F_{ISAM}(\mathbf{H}_i)|}{\sigma_{obs}(\mathbf{H}_i)} \right)^2. \qquad (3)$$

The results are illustrated in Fig. 7 and Table 1. The figure shows that *FullProf* provides estimated standard uncertainties that are substantially smaller than those of *Jana2006* and *GSAS*. The tendency is especially pronounced for the low-order structure factors. The low σ_{obs} from *FullProf* leads to very high S^2 values, whereas the weighting schemes of *Jana2006* and *GSAS* are quite similar (although *Jana2006* has marginally higher significance at low order). The J1–3 refinements produce the lowest values of S^2, whereas those of the G1–2 and F1–3 refinements are of similar magnitude. The high S^2 values for the G1–2 refinements are due to the inferior fit between model and data, rather than low standard uncertainties. The inconsistency in estimating σ_{obs} in the Rietveld programs comprises a serious problem in the utilization of the MEM for PXRD data. This problem is avoided in single-crystal data, where the σ_{obs} on the structure factors typically are derived from calculating the variance of a set of equivalent measurements. The comparison clearly shows that some kind of post-analysis of the σ_{obs} could lead to improved MEM EDDs.

The effect of erroneously estimated σ_{obs} on MEM EDDs can be deduced from the standard MEM stopping criterion, $\chi^2_{aim} = 1$, which is motivated by the expectation value of $|F_{obs}(\mathbf{H}) - F_{true}(\mathbf{H})|/\sigma_{obs}(\mathbf{H})$ being equal to 1. If MEM iterations are set to converge at $\chi^2_{aim} = 1$, the corresponding MEM EDD will be over-fitted if the applied σ_{obs} are smaller than the true values and under-fitted if they are too large. However, this simple picture gets substantially more complicated when considering some of the intrinsic MEM effects. Firstly, the standard stopping criterion is only approximate, not accounting for the bias of F_{MEM} towards F_{obs}. Hence, the point of convergence is theoretically characterized by an averaged
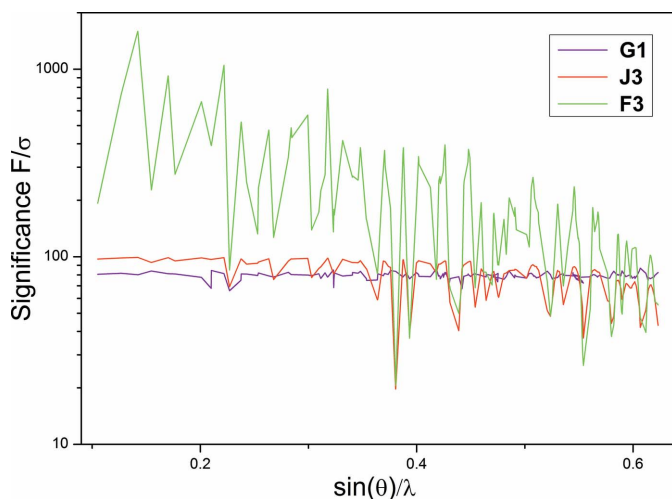
Figure 7
The significance distribution for the best refinement in each of the three Rietveld programs plotted on a logarithmic scale.

value of $|F_{obs}(\mathbf{H}) - F_{MEM}(\mathbf{H})|/\sigma_{obs}(\mathbf{H})$ smaller than 1 (Skilling, 1989). In the application of the MEM to low-temperature single-crystal X-ray diffraction data of a series of amino acids and tripeptides, the optimal value of χ^2_{aim} was found to vary between 0.31 and 1.31 (van Smaalen & Netzel, 2009). The values larger than 1 can be explained by inappropriate scaling of σ_{obs}. Secondly, the property of MEM to fabricate the flattest EDD compatible with the diffraction data causes non-random residuals, $[F_{obs}(\mathbf{H}) - F_{MEM}(\mathbf{H})]/\sigma_{obs}(\mathbf{H})$, which are dominated by a few strong low-order reflections denoted outliers (Jauch & Palmer, 1993; Iversen *et al.*, 1995; Iversen, Jensen & Danielsen, 1997). The remaining reflections are over-fitted in order to meet the convergence criterion. This problem can be reduced by employing different weighting schemes within the C_F constraint (de Vries *et al.*, 1994; Iversen *et al.*, 1995; Iversen, Jensen & Danielsen, 1997), or by utilizing a constraint based on higher-order moments of the Gaussian error distribution than the second moment represented in the C_F constraint (Palatinus & van Smaalen, 2002). Overall, the intrinsic MEM bias can be very similar to the effects arising from inaccurate estimation of σ_{obs}, and in fact corrections performed on σ_{obs} may absorb intrinsic MEM errors.

In the least-squares method the solution is independent of the scale of the uncertainties on the data points. One can rescale the σ_{obs} based *e.g.* on the goodness of fit from the ISAM model, and then use rescaled σ_{obs} in the MEM calculations. However, such a rescaling merely corresponds to changing the stopping criterion of the MEM, *i.e.* $\chi^2_{aim} = 1c^2$ or $\sigma(\mathbf{H}) = c\sigma(\mathbf{H})_{program}$ where c is an arbitrary constant. Thus, determination of an appropriate scale for the σ_{obs} corresponds to determining an optimal value for χ^2_{aim}.

4.2. Choice of χ^2_{aim}

Hofmann and co-workers proposed an approach for determining the optimum value of χ^2_{aim} based on assessments of the MEM deformation and residual density maps (Hofmann *et al.*, 2007). However, published results utilizing this approach are exclusively based on single-crystal data measured at low temperatures (20–23 K) and with high resolution $[\sin(\theta)/\lambda \simeq 1.08–1.10 \text{ Å}^{-1}]$ on molecular crystals containing light-atom systems, *e.g.* L-alanine and trialanine (Destro *et al.*, 1988; Rödel *et al.*, 2006; Hofmann *et al.*, 2007; van Smaalen & Netzel, 2009). In the present work, we study a metal hydride and for this structure it is not clear what the density should be in the internuclear regions since there is no well defined molecular 'envelope'. In addition, the Ga atom is much heavier than the atoms in organic systems and the study is based on PXRD data at much lower resolution (0.62 Å^{-1}). Consequently, it is impossible to unambiguously distinguish between real electron density and noise in these maps.

Instead we apply an alternative approach for the optimization of χ^2_{aim} based on the residual density analysis scheme developed by Meindl & Henn (2008) in the case of multipole refinements. Within this scheme the optimum value of χ^2_{aim} is obtained when the residual density has the most narrow and parabolic fractal dimension distribution. At too large values of

Table 5
Residual density descriptors for the fractal dimension distributions of F3 depicted in Fig. 8.

The total amount of residual density is quantified by $e_{gross} = (1/2) \int_V |\rho_{res}(r)| \, d^3r$ and the residual flatness by $\Delta\rho_{res} = \rho_{res,max} - \rho_{res,min}$.

F3 EDDs	$d^f(0)$	$\Delta\rho_{res}$ (e Å^{-3})	e_{gross} (e)
$\chi^2_{aim} = 0.80$	2.45	0.25	4.14
$\chi^2_{aim} = 1.00$	2.45	0.26	4.54
$\chi^2_{aim} = 1.60$	2.45	0.29	5.44
$\chi^2_{aim} = 5.00$	2.43	0.48	7.71
$\chi^2_{aim} = 11.1$	2.43	0.96	9.28
ISAM	2.43	1.08	9.60

χ^2_{aim}, systematic features arise from the under-fitting of the density, whereas at too small values of χ^2_{aim} features occur due to fitting of noise. These cases are observed in the residual density distribution e.g. as shoulders. The search for the optimum value is limited to the interval $[0, S^2]$, as the analytic ISAM EDD becomes a MEM solution at $\chi^2_{aim} = S^2$.

An example of the optimization process performed with the jnk2RDA software (Meindl & Henn, 2008) is illustrated in Fig. 8 for the F3 refinement. The MEM EDD converged at $\chi^2_{aim} = 1$ is shown in Fig. 6. As a reference point for the optimization, the residual plot of the F3 ISAM model is included. The positive residual density distribution is characterized by a round shoulder with a high fractal dimension level, where on average $F_{obs} > F_{ISAM}$. This corresponds to the bonding electrons, which are poorly described by the ISAM model. Likewise, the large shoulder of the negative residual distribution is due to regions in which $F_{obs} < F_{ISAM}$. These spatial regions have less electron density than that modelled by the ISAM attributable to physical effects such as bonding,
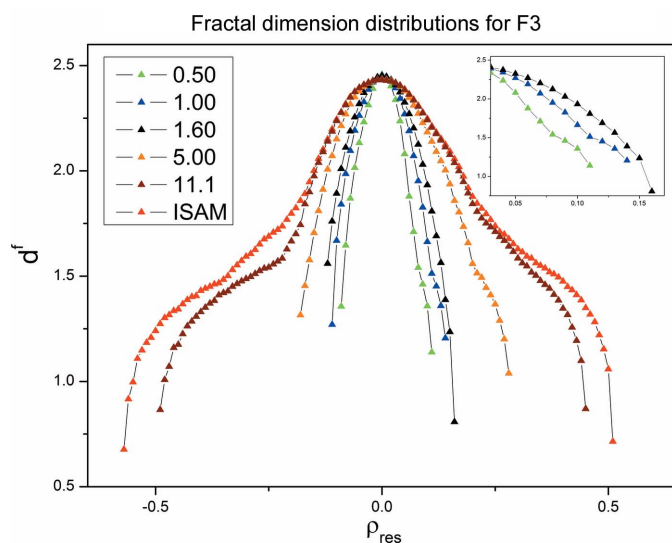
Figure 8
A series of fractal dimension distributions calculated from the F3 MEM residual densities, ρ_{res}, computed by the inverse Fourier transformation of the difference $F_{obs}(\mathbf{H}) - F_{MEM}(\mathbf{H})$. Different ρ_{res} are calculated by varying the stopping criterion, χ^2_{aim}, in the interval $[0, S^2]$; S^2 is the modified goodness-of-fit parameter defined in equation (3). A reference point is given by the fractal dimension distribution of the residual plot of the difference $F_{obs}(\mathbf{H}) - F_{ISAM}(\mathbf{H})$.

polarized density and charge transfer (Meindl & Henn, 2008). These prominent features are suppressed by MEM, as seen in the residual distribution plot obtained for the EDD converged at $\chi^2_{aim} = 1$; however, features are still present in terms of a weak shoulder on the positive residual distribution. Thus, a search for a more parabolic fractal dimension distribution is initiated. Besides visual inspection of the distributions, the accuracy of the search is quantified by fitting a parabolic function, $f(x) = c_1 x^2 + c_2$, to each of them. Thereby, a coefficient of determination, R^2, is obtained, which is utilized as a quantitative estimate of how Gaussian the residual density distributions are. In the case of F3, MEM EDDs with a Gaussian error distribution ($R^2 \simeq 0.99$) are found for χ^2_{aim} values ranging from 1.60 to 1.90 (see Fig. 9). Within this interval, the lowest value defines the optimum value of χ^2_{aim}, since it fits the diffraction data most closely, i.e. $\chi^2_{aim} = 1.60$ is the optimal value for the F3 MEM EDD. When further increasing the stopping criterion, significant features again begin to dominate the distributions at $\chi^2_{aim} \simeq 4.0$. It can be noticed that many of the features of the ISAM fractal dimension distribution are recovered when moving towards $\chi^2_{aim} = S^2$. This is due to the application of an ISAM prior in the MEM calculations. It should also be noticed that the modification of the F3 standard uncertainties by a scale factor of $1.60^{1/2}$ results in an S^2 value of 6.92 that remains considerably higher than those obtained with the J1–3 refinements (Table 1). However, by altering the stopping criterion to the optimum value as determined by the residual distributions, features due to over-fitting are minimized in the MEM EDD (see Fig. 10).

A quantitative description of the optimization process for the F3 MEM EDD is shown in Table 5, which lists the residual descriptors defined by Meindl and Henn. First of all, it is seen that $d^f(0)$ of the optimized MEM EDD is slightly increased compared to the ISAM. This is in accordance with the example demonstrated by Meindl and Henn, in which a multipole refinement raised the value of $d^f(0)$ by 0.02 relative
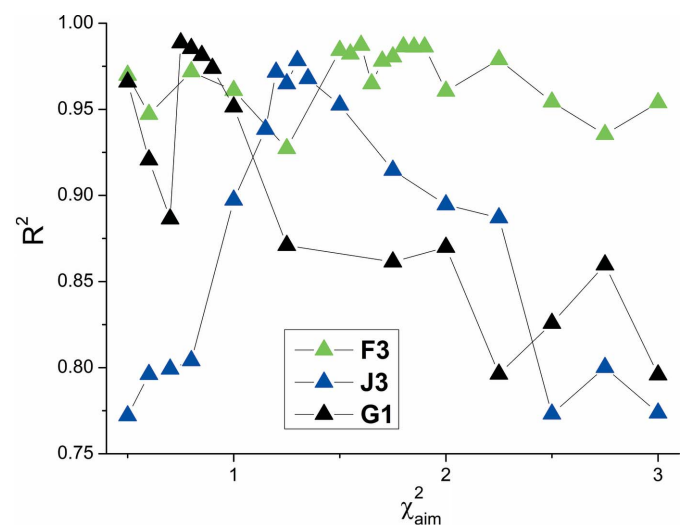
Figure 9
Coefficients of determination, R^2, obtained by fitting fractal dimension distributions to a parabolic function, $f(x) = c_1 x^2 + c_2$.

Table 6
The optimized χ^2_{aim} value, $(\chi^2_{\text{aim}})_{\text{opt}}$, and the rescaled, modified goodness of fit, $(S^2)_{\text{opt}}$.
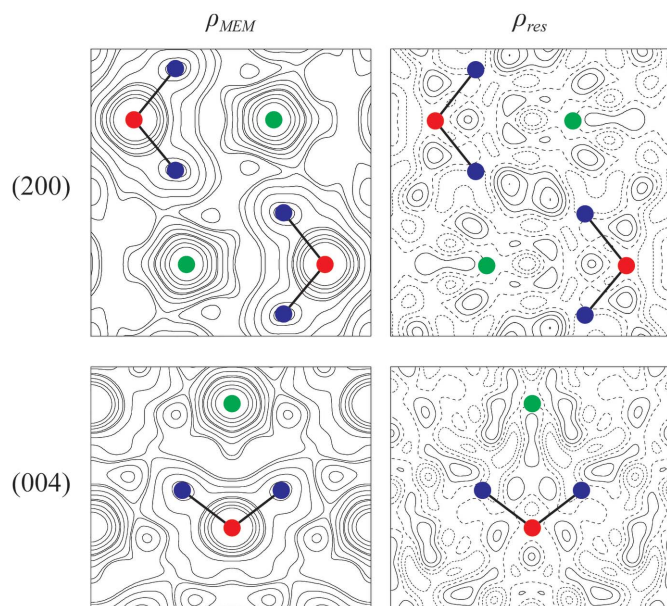
Definition of the MEM agreement factors is provided in Table 1. Atomic charges (e), the density at the BCPs (e Å^{-3}) obtained from topological analysis of optimized MEM EDDs as well as residual density descriptors, $\Delta\rho_{\text{res}}$ (e Å^{-3}), e_{gross} (e) and $d^f(0)$.

	F1	F2	F3	J1	J2	J3	G1	G2
$(\chi^2_{\text{aim}})_{\text{opt}}$	1.30	1.80	1.60	1.45	1.25	1.30	0.75	1.70
$(S^2)_{\text{opt}}$	15.5	10.9	6.92	2.59	2.66	2.33	15.3	6.47
R_{MEM}	0.56	0.63	0.58	1.28	1.20	1.20	0.92	1.34
R_{wMEM}	0.38	0.45	0.42	1.50	1.39	1.42	1.09	1.65
Topological analysis								
Q_{Na}	0.71	0.75	0.54	0.74	0.72	0.72	1.06	0.95
Q_{Ga}	0.88	0.61	0.76	0.58	0.55	0.47	1.75	1.50
Q_{H1}	-0.10	-0.33	-0.19	-0.33	-0.31	-0.30	-0.48	-0.46
Q_{H2}	-0.29	-0.35	-0.37	-0.31	-0.31	-0.29	-0.41	-0.59
Q_{NaGaH4}	0.79	0.00	0.18	0.05	0.03	0.00	1.03	0.36
$\rho^{\text{Ga}-\text{H1}}_{\text{BCP}}$	0.75	0.71	0.71	0.62	0.62	0.63	0.85	0.73
$\rho^{\text{Ga}-\text{H2}}_{\text{BCP}}$	0.57	0.58	0.55	0.49	0.50	0.49	0.53	0.64
Residual descriptors								
$d^f(0)$	2.46	2.46	2.45	2.41	2.41	2.40	2.38	2.40
$\Delta\rho_{\text{res}}$	0.29	0.33	0.29	0.71	0.67	0.67	0.47	0.62
e_{gross}	4.97	5.55	5.44	11.29	10.71	10.84	8.96	11.18

to the ISAM. The slight increase in $d^f(0)$ disappears when χ^2_{aim} is further increased, since the MEM solution approaches the ISAM. As anticipated, the values of ρ_o and e_{gross} grow as χ^2_{aim} increases, since larger differences between F_{MEM} and F_{obs} are gradually enabled.

Intrinsic MEM effects (*i.e.* MEM bias) were briefly discussed above, where it was implied that these effects could be resolved by re-scaling the uncertainties or changing χ^2_{aim}. When determining the optimum χ^2_{aim}, a correction for F_{MEM} bias towards F_{obs} is automatically performed. However, this scheme only reduces the effect of non-random residuals in the instances where the optimum χ^2_{aim} is smaller than 1. Thus, in the present optimization process where the optimum value of χ^2_{aim} equals 1.60, the size of the outliers will increase, but the distribution has become more Gaussian as demonstrated in Fig. 8.

4.3. Optimal electron densities

All MEM EDDs based on the refinements with varying background approximation (Table 1) have been optimized applying the procedure described in the previous section with F3 as an example. Examples of the optimization process for *Jana2006* and *GSAS* are illustrated in Fig. 9 utilizing J3 and G1. The remaining optimization processes are demonstrated in the supplementary materials. In contrast to the F3 optimization, the optimum χ^2_{aim} value of both refinements is defined by a clearly isolated maximum in the coefficient of determination curve. The overall result is optimal χ^2_{aim} values located in the interval between 1.25 and 1.80 for all refinements except G1, for which a value lower than the standard value of 1 is determined (see Table 6). Remembering that especially for the strong low-order reflection the σ_{obs} of J1–3 are considerably larger than those of F1–3 (Fig. 7), it is quite surprising that the optimum χ^2_{aim} values of J1–3 and F1–3 are of similar magnitude. As a consequence, the optimized J1–3 MEM EDDs are more loosely constrained to the diffraction data and stronger features are allowed in their residual densities. The latter is elaborated by considering the residual density descriptors listed in Table 6. Herein, the poor quality of the J1–3 residual

ρ_{MEM} ρ_{res}

(200)

(004)

Figure 10
The optimized F3 MEM EDD ($\chi^2_{\text{aim}} = 1.60$) in the (200) and (004) sections of NaGaH$_4$; Ga—H1 is observed in the (200) section, whereas Ga—H2 is seen in (004). The contour levels of ρ_{MEM} are defined by $2^x \times 10^y$; $x = 0, 1, 2, 3$ and $y = -2, -1, 0$, whereas the contour levels of ρ_{res} are at 0.04 e Å^{-3}. Ga (red), Na (green) and H (blue).

EDDs is clearly demonstrated by the two descriptors, $\Delta\rho_{res}$ and e_{gross}, which in the case of J1–3 are approximately twice as large compared to F1–3. Their values are even similar to those of G1–2. However, the similarity of F_{obs} extracted from F1–3 and J1–3 (Fig. 3 and Table 2) implies that the residual EDDs of J1–3 can be improved if their weighting scheme is modified to resemble that of F1–3, *i.e.* low-order reflections ought to have more weight (see Fig. 7). Additional support is provided by the difference distribution, $F_{obs}(\mathbf{H}) - F_{MEM}(\mathbf{H})$, which shows that the low-order reflections deviate considerably more for J1–3. Thus, the employment of *ad hoc* weighting schemes within the C_F constraint (de Vries *et al.*, 1994; Iversen *et al.*, 1995; Iversen, Jensen & Danielsen, 1997) or higher-order moments of the Gaussian error distribution (Palatinus & van Smaalen, 2002) may be viable options for improving the J1–3 EDDs. The similarity of the G1 and J3 significance distribution (Fig. 7) indicates that this applies to G1–2 as well. Conversely, the above-mentioned weighting schemes would have a lesser impact on F1–3.

Topological analysis was carried out on the optimized EDDs (Bader, 1994) and the main results are provided in Table 6. Compared with the analysis of the standard MEM EDDs analysed in Table 1, significant improvements are found, especially for the *FullProf* refinements. The optimized F2 EDD complies completely with electroneutrality, whereas only 0.4% of the electrons are not accounted for in the optimized F3 EDD, in contrast to 1.2% for the standard F3 EDD. It should be noted that a slight increase in the optimized χ^2_{aim} of F3 results in a MEM EDD with a maintained Gaussian error distribution and improved electroneutrality. Therefore, if electroneutrality is utilized as an additional χ^2_{aim} selection criterion, the optimum χ^2_{aim} value for F3 will increase from 1.60 to 1.80. At this point, more electrons are allocated to H1 (Q_{H1} = −0.28 compared to −0.19) as the further reduced overfitting has increased the volume of its atomic basin. In the case of J1–3, significant improvements are only observed for the J1 EDD, for which Q_{NaGaH4} is reduced from 0.25 to 0.05 e. The optimized J2–3 EDDs are similar to the standard ones; considerable alterations are only observed for Q_{Ga}, which is reduced by 0.07 and 0.10 e for J2 and J3, respectively. The optimized G1–2 EDDs differ substantially from their standard counterparts; however, only G2 has improved its electroneutrality: Q_{NaGaH4} is reduced from 1.27 to 0.36. As the G1 optimization is the sole case with an optimum χ^2_{aim} value smaller than 1, this demonstrates that electroneutrality for these MEM EDDs generally improves with increasing χ^2_{aim}.

For the F1–3 and J1–3 EDDs, the modifications in the vicinity of H1 are the general cause for the electroneutrality enhancements, and their optimized ρ_{BCP}^{Ga-H} values are similar to those of the standard EDDs; the maximal difference is 0.03 e Å^{-3}. Concerning electroneutrality of the G1–2 EDDs, the picture is reversed as the main modifications occur in the atomic basins of Na, Ga and H2. Their optimized ρ_{BCP}^{Ga-H} values are slightly altered compared to their standard counterparts; the maximal difference is 0.06 e Å^{-3}.

5. Conclusion

The use of the maximum entropy method for calculation of EDDs was examined based on structure factors extracted from synchrotron PXRD data with the three commonly used Rietveld refinement programs: *GSAS*, *FullProf* and *Jana2006*. Only *Jana2006* fulfils the basic requirement of producing an output file with structure factors on an absolute scale corrected for anomalous dispersion. In the case of *FullProf* and *GSAS* it is necessary to carry out a post-treatment of the data to obtain values suitable for MEM calculations. It was shown that background modelling using linear interpolation can be sufficient for determining MEM EDDs of high quality, but further improvements are obtainable when linear interpolation is combined with a smoothing function or scheme. For the present data the available background options in *GSAS* are clearly inferior to *FullProf* and *Jana2006*. Since the modelling of the background is found to be critical for obtaining high-quality MEM EDDs we propose that further efforts are invested in data collections to lower the background as much as possible.

The three Rietveld programs provide very different estimates of the standard uncertainties on the structure factors. This comprises a serious problem in MEM calculations, since the standard uncertainties are used directly in the central MEM equation. In order to overcome this problem the residual distribution analysis developed by Meindl & Henn (2008) for multipole modelling was used to characterize features and noise, and the method provides an effective way of selecting the optimum stopping criteria in MEM calculation. The optimized EDDs are primarily characterized by modifications in the low-density region, which especially for the *FullProf* refinements leads to a considerably improved accordance with electroneutrality. The differences in the programs' weighting schemes imply that the employment of alternative weighting schemes within the C_F constraint or higher-order moments of the Gaussian error distribution have a more pronounced impact in *Jana2006* and *GSAS*.

References

Bader, R. F. W. (1994). *Atoms in Molecules: A Quantum Theory*. Oxford University Press.
Bagautdinov, B., Luedecke, J., Schneider, M. & van Smaalen, S. (1998). *Acta Cryst.* B**54**, 626–634.
Bakum, S. I. & Ereshko, S. F. (1977). *Zh. Neorg. Khim.* **22**, 655–659.
Bentien, A., Palmqvist, A. E. C., Bryan, J. D., Latturner, S., Stucky, G. D., Furenlid, L. & Iversen, B. B. (2000). *Angew. Chem. Int. Ed.* **39**, 3613–3616.
Buchter, F., Lodziana, Z., Remhof, A., Mauron, P., Friedrichs, O., Borgschulte, A., Zuttel, A., Filinchuk, Y. & Palatinus, L. (2011). *Phys. Rev. B*, **83**, 064107.
Coppens, P. (1967). *Science*, **158**, 1577–1579.

Destro, R., Marsh, R. E. & Bianchi, R. (1988). *J. Phys. Chem.* **92**, 966–973.

Dinnebier, R. E., Schneider, M., van Smaalen, S., Olbrich, F. & Behrens, U. (1999). *Acta Cryst.* B**55**, 35–44.

Fischer, A., Tiana, D., Scherer, W., Batke, K., Eickerling, G., Svendsen, H., Bindzus, N. & Iversen, B. B. (2011). *J. Phys. Chem. A*, **115**, 13061–13071.

Fischer, P., Frey, G., Koch, M., Konnecke, M., Pomjakushin, V., Schefer, J., Thut, R., Schlumpf, N., Burge, R., Greuter, U., Bondt, S. & Berruyer, E. (2000). *Physica B*, **276**, 146–147.

Gilmore, C. J. (1996). *Acta Cryst.* A**52**, 561–589.

Hansen, N. K. & Coppens, P. (1978). *Acta Cryst.* A**34**, 909–921.

Herbst, J. F., Hector, L. G. & Wolf, W. (2010). *Phys. Rev. B*, **82**, 024110.

Hofmann, A., Netzel, J. & van Smaalen, S. (2007). *Acta Cryst.* B**63**, 285–295.

Irodova, A. V., Somenkov, V. A., Bakum, S. I. & Kuznetsova, S. F. (1989). *Z. Phys. Chem. Neue Folge*, **163**, 239–242.

Iversen, B. B., Jensen, J. L. & Danielsen, J. (1997). *Acta Cryst.* A**53**, 376–387.

Iversen, B. B., Larsen, F. K., Figgis, B. N. & Reynolds, P. A. (1997). *J. Chem. Soc. Dalton Trans.* pp. 2227–2240.

Iversen, B. B., Nielsen, S. K. & Larsen, F. K. (1995). *Philos. Mag. A*, **72**, 1357–1380.

Jauch, W. (1994). *Acta Cryst.* A**50**, 650–652.

Jauch, W. & Palmer, A. (1993). *Acta Cryst.* A**49**, 590–591.

Larson, A. C. & Von Dreele, R. B. (1994). *GSAS*. Report LAUR 86-748. Los Alamos National Laboratory, New Mexico, USA.

Macchi, P., Iversen, B. B., Sironi, A., Chakoumakos, B. C. & Larsen, F. K. (2000). *Angew. Chem. Int. Ed.* **39**, 2719–2722.

Meindl, K. & Henn, J. (2008). *Acta Cryst.* A**64**, 404–418.

Nishibori, E., Sunaoshi, E., Yoshida, A., Aoyagi, S., Kato, K., Takata, M. & Sakata, M. (2007). *Acta Cryst.* A**63**, 43–52.

Nishibori, E., Takata, M., Kato, K., Sakata, M., Kubota, Y., Aoyagi, S., Kuroiwa, Y., Yamakata, M. & Ikeda, N. (2001). *Nucl. Instrum. Methods Phys. Res. A*, **467**, 1045–1048.

Noritake, T., Towata, S., Aoki, M., Seno, Y., Hirose, Y., Nishibori, E., Takata, M. & Sakata, M. (2003). *J. Alloys Compd*, **356**, 84–86.

Nozik, Y. Z., Kuklina, E. S., Bliznyuk, N. A. & Borisov, S. V. (1991). *Kristallografiya*, **36**, 57–61.

Overgaard, J., Schiøtt, B., Larsen, F. K. & Iversen, B. B. (2001). *Chem. Eur. J.* **7**, 3756–3767.

Overgaard, J., Schiott, B., Larsen, F. K., Schultz, A. J., MacDonald, J. C. & Iversen, B. B. (1999). *Angew. Chem. Int. Ed.* **38**, 1239–1242.

Palatinus, L. & van Smaalen, S. (2002). *Acta Cryst.* A**58**, 559–567.

Petricek, V., Dusek, M. & Palatinus, L. (2006). *Jana2006*. Institute of Physics, Praha, Czech Republic.

Press, W., Teukolsky, S., Vetterling, W. & Flannery, B. (1992). *Numerical Recipes.* Cambridge University Press.

Rietveld, H. M. (1969). *J. Appl. Cryst.* **2**, 65–71.

Rödel, E., Messerschmidt, M., Dittrich, B. & Luger, P. (2006). *Org. Biomol. Chem.* **4**, 475–481.

Rodriguez-Carvajal, J. (1993). *Physica B*, **192**, 55–69.

Sakata, M. & Sato, M. (1990). *Acta Cryst.* A**46**, 263–270.

Samy, A., Dinnebier, R. E., van Smaalen, S. & Jansen, M. (2010). *Acta Cryst.* B**66**, 184–195.

Skilling, J. (1989). *Maximum Entropy and Bayesian Methods*, **36**, 45–52.

Smaalen, S. van & Netzel, J. (2009). *Phys. Scr.* **79**, 1–9.

Smaalen, S. van, Palatinus, L. & Schneider, M. (2003). *Acta Cryst.* A**59**, 459–469.

Snyder, G. J., Christensen, M., Nishibori, E., Caillat, T. & Iversen, B. B. (2004). *Nat. Mater.* **3**, 458–463.

Spackman, M. A. (1991). *Acta Cryst.* A**47**, 420–427.

Svendsen, H., Overgaard, J., Busselez, R., Arnaud, B., Rabiller, P., Kurita, A., Nishibori, E., Sakata, M., Takata, M. & Iversen, B. B. (2010). *Acta Cryst.* A**66**, 458–469.

Takata, M., Nishibori, E. & Sakata, M. (2001). *Z. Kristallogr.* **216**, 71–86.

Takata, M., Umeda, B., Nishibori, E., Sakata, M., Saito, Y., Ohno, M. & Shinohara, H. (1995). *Nature (London)*, **377**, 46–49.

Thompson, P., Cox, D. E. & Hastings, J. B. (1987). *J. Appl. Cryst.* **20**, 79–83.

Toby, B. H. (2001). *J. Appl. Cryst.* **34**, 210–213.

Vajeeston, P., Ravindran, P., Vidya, R., Fjellvag, H. & Kjekshus, A. (2004). *Cryst. Growth Des.* **4**, 471–477.

Von Dreele, R. B. (1994). *FPrime*. Los Alamos National Laboratory, New Mexico, USA.

Vries, R. Y. de, Briels, W. J. & Feil, D. (1994). *Acta Cryst.* A**50**, 383–391.

Vries, R. Y. de, Briels, W. J. & Feil, D. (1996). *Phys. Rev. Lett.* **77**, 1719–1722.